*Materials Science-Poland, 39(2), 2021, pp. 285-297*
*http://www.materialsscience.pwr.wroc.pl/*
*DOI: 10.2478/msp-2021-0024*

# 2D and 3D numerical simulation of fatigue crack growth path and life predictions of a linear elastic

Abdullateef H. Bashiri[1,*]

[1]Department of Mechanical Engineering, Jazan University, P. O. Box 114, Jazan 45142, Saudi Arabia

This paper describes implementation of the finite element method (FEM) to investigate crack growth problems in linear elastic fracture mechanics and the correlation of results with experimental and numerical data. The approach involved using two different software to compute stress intensity factors (SIFs), the crack propagation trajectory, and fatigue life estimation in two and three dimensions. According to the software, crack modeling might be run in various ways. The first is a developed source code program written in the Visual Fortran language, while the second is the widely used ANSYS Mechanical APDL 19.2 software. The fatigue crack propagation trajectory and the corresponding SIFs were predicted using these two software programs. The crack direction was investigated using the maximum circumferential stress theory, and the finite element (FE) analysis for fatigue crack growth was done for both software based on Paris's law. The predicted results in both software demonstrated the influence of holes on the crack growth trajectory and all associated stresses and strains. The study's findings agree with other experimental and numerical crack propagation studies presented in the literature that reveal similar crack propagation trajectory observations.

Keywords: *ANSYS mechanical, smart crack growth, stress intensity factors, Linear Finite Element Method (LEFM), source code, hole influence*

## 1. Introduction

The prediction of curvilinear fatigue and fracture is a topic for ongoing research. A mathematical study has provided few curved crack path propagation solutions [1, 2], but experimental results can be accurately reproduced in computer ways. The main objective of fracture mechanics is to determine whether or not a structure will fail based on a crack. Crack analysis should start from field stresses in the crack tip, evaluated by the equivalent stress intensity factor (Keq). By comparing the Keq value to a peculiar characteristic of each material called fracture toughness or threshold stress intensity factor, it is possible to determine whether or not a crack member would fail when subjected to static or fatigue loading, respectively. In general, cracks' initiation and propagation must be associated with stress intensity factors (SIFs) in a complicated state [3–7]. The prediction of curvilinear fatigue and fractures remains a topic of ongoing research. Few curved crack path propagation solutions were obtained by mathematical analysis, but computational approaches can accurately reproduce experimental results [8–10]. Numerical simulations typically calculate the energy derivatives in the first order concerning crack length or the equivalent SIFs. Meanwhile, new approaches and methods in several areas of study have been suggested and developed rapidly, including the finite element method (FEM), discrete element method (DEM) [11–13], element free Galerkin (EFG) method [14], extended finite element method (XFEM) [15–18], cohesive element method [19, 20], and phase-field method [21]. Nevertheless, as a versatile method to simulate crack propagation, the FEM is still prevalent. In general, the propagation of an internal crack in the engineering practice is essential because of its significant effect on the quality and stability of engineering structures. Thus, it is important to predict the crack propagation path for safety and reliability of engineering structures. Therefore, in many industries, the accurate estimation of the crack path and fatigue life estimation is of pri-

* E-mail: absheiri@jazanu.edu.sa

© 2021. This is an open access article distributed under the Creative Commons Attribution-NonCommercial-NoDerivatives 4.0 License. (http://creativecommons.org/licenses/by-nc-nd/4.0/)

mary importance in terms of reliability. In various applications, such as aerospace manufacturing and the aviation industry, experimental studies are necessary for fatigue analysis. However, due to high costs, an accurate computational approach is required for crack propagation analysis to prognosticate the direction of crack growth and fatigue life in both static and dynamic loading conditions [22–24]. The failure is related to (a) the presence of flaws such as interfaces and cracks and (b) the nature of loads that fluctuate. Cracks tend to initiate and propagate when subjected to fluctuating loads until the structure does not bear the load contributing to complete failure. These cracks are considered to be fatigue cracks, and the expected fatigue life is one of the most significant parameters to determine the structure's safety. It can be computed by adding the number of loading cycles needed to propagate the fatigue crack and lead to failure. The calculation of the growth rate of the crack is generally based on the relationship within the range of SIFs and the crack geometry. One way to predict SIFs is using computational methods such as the XFEM. The XFEM introduced by Belytschko and Black in 1999 [25] was widely used in novel investigations. It is based on the conventional finite element (FE) framework. It uses a novel displacement feature allowing discontinuities to happen, to defeat the need to re-mesh continuously during the crack tip development process [26]. Extended work was offered to promote practical models to estimate the fatigue failure and fatigue growth to subdue fatigue failures. Several experimental tests are proposed [27, 28], but the performance of the experimental procedures is usually time-consuming and costly. An effective way to reduce the laboratory work, time, and costs is to incorporate a simulation methodology to including the numerical analysis. Many fatigue crack problems identified to date by the literature use different computational approaches in simulation for simplistic and complicated geometries in 2D and 3D [10, 22, 29–35]. In this paper, the ANSYS APDL 19.2 is used to precisely predict the mixed-mode stress intensity and correlated fatigue response for seven specimens of the modified compact tension specimen (MCTS). In particular, three methods were widely used to illustrate the fatigue estimation of different specimens: (a) the fracture mechanics based on Paris and Erdogan [36]; (b) the method of strain-life independently proposed by Coffin [37]; and (c) the method of stress-life proposed by Wöhler [38]. The first approach was employed in this study for predicting fatigue life by which the crack tip can be described separately by the SIFs. The primary motivation for this study was to perform a proper comparison of the predicted results for crack propagation parameters using the author's 2D software and the 3D ANSYS software as an alternate tool for simulating fatigue crack growth subjected to mixed-mode loading. The computational time to simulate the crack propagation in the developed 2D program is approximately one-fifth compared with the ANSYS modeling for the same geometry and mesh density.

## 2. Mixed mode fatigue life evaluation procedure using ANSYS MECHANICAL APDL 19.2

There are three types of cracks that ANSYS can model: arbitrary, semi-elliptical, and pre-meshed. The Separating Morphing and Adaptive Remeshing Technology (SMART) uses the crack front in the pre-meshed crack approach, and the stress intensity factor is the failure criteria. The rendered node sets will distribute to the front of the crack, as well as to the top and bottom of the crack. By employing SIFs as the failure criteria, the front of the crack is represented in the pre-meshed crack process used by the "Smart Crack Growth" simulation tool. SMART automatically updates the mesh from crack geometry modifications based on crack propagation on each solution level, eliminating the need for long pre-processing sessions. The sphere of influence method around the crack tip that goes through the thickness can be used to improve the mesh around the crack tip. The geometric regions to be described are the crack tip, the crack's top surface, and the crack's bottom surface. Instead, each of these regions is associated with a node-set to be used for analysis. The ANSYS MECHANICAL APDL 19.2 software considers mixed-mode loading where the maximum circumferential stress cri-

terion is implemented. The following is the formula for the direction of crack propagation [32, 33]:

$$\theta = \cos^{-1}\left(\frac{3K_{II}^2 + K_I\sqrt{K_I^2 + 8K_{II}^2}}{K_I^2 + 9K_{II}^2}\right) \quad (1)$$

where $K_I$ = Max $K_I$ during cyclic loading and $K_{II}$ = Max $K_{II}$ during cyclic loading. The two possibilities for crack growth direction are visualized in Figure 1.

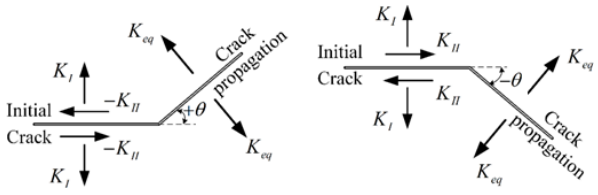



Fig. 1. Crack propagation angle according to the second mode of SIFs **(A)** $K_{II} > 0$ **(B)** $K_{II} < 0$.

In ANSYS Mechanical, the simulation of crack propagation is restricted to region II of the typical fatigue crack growth graph based on Paris' law that can be represented as:

$$\frac{da}{dN} = C(\Delta K_{eq})^m \quad (2)$$

From Eq. (2), for a crack increment, the number of fatigue life cycles may be predicted as:

$$\int_0^{\Delta a} \frac{da}{C(\Delta K_{eq})^m} = \int_0^{\Delta N} dN = \Delta N \quad (3)$$

The equivalent range for the stress intensity factor formula can be found as follows [39]:

$$\Delta K_{eq} = \tfrac{1}{2}\cos\tfrac{\theta}{2}\left[(\Delta K_I(1+\cos\theta)) - 3\Delta K_{II}\sin\theta\right] \quad (4)$$

where $\Delta K_I$ = the stress intensity factor range in mode I loading and $\Delta K_{II}$ = the stress intensity factor range in mode II loading. The ANSYS flow chart is shown in Figure 1.

## 3. Developed program procedure

The developed program is a Visual Fortran-based simulation for analyzing two dimensional crack propagation processes under LEFM conditions. This program uses the FE approach to estimate the propagation of quasi-static fatigue cracks in 2D components, taking into account the fracture's mechanical boundary conditions. The adaptive mesh FE method includes four main components for crack trajectory simulation: the mesh optimization technique, the crack criterion, the direction criterion, and the crack propagation strategy. The mesh refinement can be controlled by the characteristic scale of each element, which the error estimator predicts. The step by step analysis is disturbed, and a new FE model is constructed when the error reaches a stated, cumulative error at some point throughout the simulation. Within the initial boundary conditions, the system refines the mesh as needed. After the new mesh is generated, the solution variables (displacement, stresses, strains) are mapped from the previous mesh into the newly created mesh. The analysis is then repeated and continued until the errors exceed the pre-decided number. SIFs are employed in LEFM as fracture criteria. The maximum circumferential stress theory [40], maximum energy release theory [41], and minimum strain-energy density theory [42] are just a few of the methodologies used to predict a crack's propagation direction. The maximum circumferential stress theory has been used in the developed program as a direction criterion.

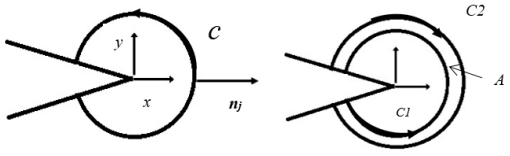
### 3.1. SIFs method

The most successful engineering implementation of fracture mechanics is crack growth laws based on stress intensity factor ranges [43]. Irwin [44] defined the stress intensity factor, abbreviated as K, as a mechanical parameter that represents the state of stress at a crack point. For various common crack configurations, many analytical solutions for the SIFs were developed. On the other hand, these analytical solutions are restricted to simple crack geometries and loading conditions [2]. Small-sized yield requirements were implemented [45], which established a J-integral methodology for investigating the nonlinear behavior of the material [46]. The equivalent domain integral methodology replaces the finite-

size domain with a divergence theorem by integration along the contour for FEM. The integral independent contour of the trajectory is as follows [46]:

$$J = \int_C \left( W n_1 - \sigma_{ij} n_j \frac{\partial u_i}{\partial x} \right) ds \tag{5}$$

where $W$ is the strain-energy density, $\sigma_{ij}$ are the stresses, $u_i$ is the local $i$ axis displacement, $s$ is the contour arc length, and $n_j$ is the outward unit normal to the contour $C$ around the crack tip (Figure 2A).




(A) (B)

Fig. 2. **(A)** Crack tip in an arbitrary contour, **(B)** J-integral area.

For 2D structures, the contour integral i is replaced by area integral (Figure 2B). Then, Eq. (5) is modified as:

$$J_k = -\int_A \left[ W \frac{\partial q}{\partial x} - \sigma_{ij} \frac{\partial u_i}{\partial x} \frac{\partial q}{\partial x} \right] dA \tag{6}$$
$$-\int_A \left[ \frac{\partial W}{\partial x} - \frac{\partial}{\partial x} \left( \sigma_{ij} \frac{\partial u_i}{\partial x} \right) \right] q dA - \int_s t_i \frac{\partial u_i}{\partial x} q ds$$

The step by step procedure of the developed program software is illustrated in Figure 3. The details of these steps are explained in the literature [29, 45, 47–50]. The adaptive mesh refinement was explained in detail by Bashiri and Alshoaibi [45].

In LEFM simulation, the J-integral by definition takes into account translational mechanical energy balance in the tip region of the crack along x axis. Eq. (6) simplifies the computation of mode I and II of SIFs but they do not compute $K_I$ and $K_{II}$ separately for multiple load conditions. In these cases, the following integral should be considered [50]:

$$J_k = -\int_A \left[ W \frac{\partial q}{\partial x_k} - \sigma_{ij} \frac{\partial u_i}{\partial x_k} \frac{\partial q}{\partial x_j} \right] dA \tag{7}$$

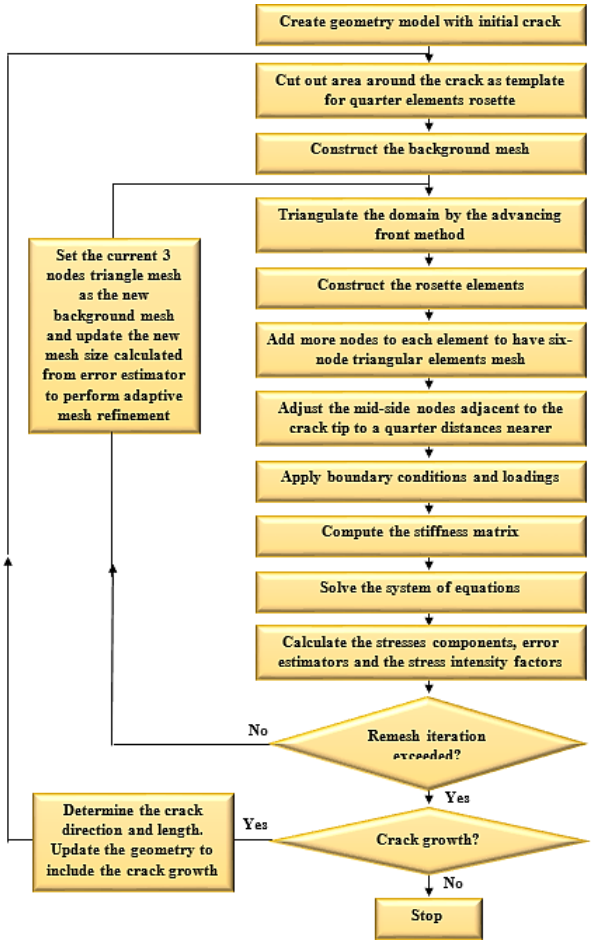



Fig. 3. Computational procedure of the fatigue crack growth developed program.

$$-\int_A \left[ W \frac{\partial q}{\partial x_k} - \sigma_{ij} \frac{\partial}{\partial x_j} \left( \frac{\partial u_i}{\partial x_k} \right) \right] q dA$$
$$-\int_s t_i \frac{\partial u_i}{\partial x_k} q ds$$

where $k$ represents the crack tip's index. The SIFs can be calculated using one of the following methods. The first method uses the J-integral and SIFs as:

$$J_1 = \frac{\kappa + 1}{8\mu} \left( K_I^2 + K_{II}^2 \right) \tag{8}$$
$$J_2 = -\frac{\kappa + 1}{4\mu} K_I K_{II}$$

The second method uses the relation between SIFs

and $J_1$ and $J_2$ as:

$$K_I = 0.5\sqrt{\frac{8\mu}{\kappa+1}} + \left(\sqrt{J_1 - J_2} + \sqrt{J_1 + J_2}\right) \quad (9)$$
$$K_{II} = 0.5\sqrt{\frac{8\mu}{\kappa+1}} + \left(\sqrt{J_1 - J_2} - \sqrt{J_1 + J_2}\right)$$

Where $\kappa$ is the elastic parameter defined as:

$$\kappa = \begin{vmatrix} (3-4\nu) & \text{plane stress} \\ (3-\nu)/(1+\nu) & \text{plane strain} \end{vmatrix}$$

## 3.2. Adaptive mesh refinement

Adaptive mesh refinement is an optimization method used in the field of FE mesh. The a posteriori error estimation used in this scheme is derived from the previous mesh generation. The stress error norm, also known as relative stress norm error, is used to estimate the mesh refinement error. The ratio of element norm stress error to the average standard stress error of the entire region was calculated using h-type adaptive mesh optimization. The mesh size for each element in this scheme is provided as:

$$h_e = \sqrt{2A_e}, \quad (10)$$

where $A_e$ is the triangle element area. For each element, the norm stress error is represented by:

$$\|e\|_e^2 = \int_{\Omega^e} (\boldsymbol{\sigma} - \boldsymbol{\sigma}^*)^{\mathrm{T}} (\boldsymbol{\sigma} - \boldsymbol{\sigma}^*)\, 2\mathrm{d}\Omega \quad (11)$$
$$= \int_{\Omega^e} \left( \begin{Bmatrix} \sigma_x \\ \sigma_y \\ \tau_{xy} \\ \sigma_z \end{Bmatrix} - \begin{Bmatrix} \sigma_x^* \\ \sigma_y^* \\ \tau_{xy}^* \\ \sigma_z^* \end{Bmatrix} \right)^{\mathrm{T}} \left( \begin{Bmatrix} \sigma_x \\ \sigma_y \\ \tau_{xy} \\ \sigma_z \end{Bmatrix} - \begin{Bmatrix} \sigma_x^* \\ \sigma_y^* \\ \tau_{xy}^* \\ \sigma_z^* \end{Bmatrix} \right) 2\mathrm{d}\Omega$$

However, the average norm stress error over the whole domain is represented as:

$$\|\hat{\mathrm{e}}\|^2 = \frac{1}{m} \sum_{e=1}^{m} \int_{\Omega^e} \boldsymbol{\sigma}^{\mathrm{T}} \boldsymbol{\sigma}\, 2\mathrm{d}\Omega \quad (12)$$
$$= \frac{1}{m} \sum_{e=1}^{m} \int_{\Omega^e} \begin{Bmatrix} \sigma_x \\ \sigma_y \\ \tau_{xy} \\ \sigma_z \end{Bmatrix}^{\mathrm{T}} \begin{Bmatrix} \sigma_x \\ \sigma_y \\ \tau_{xy} \\ \sigma_z \end{Bmatrix} 2\mathrm{d}\Omega$$

where $m$ is the overall number of elements in the entire domain and $\boldsymbol{\sigma}^*$ is the smoothed stress vector. The integration with the triangular isoparametric dimension will be converted in the FEM by the summation of quadratics according to the Radau rules as follows:

$$\|\mathrm{e}\|_e^2 = \int_{-1}^{1}\int_{-1}^{1} \left( \begin{Bmatrix} \sigma(\xi,\eta)_x \\ \sigma(\xi,\eta)_y \\ \tau(\xi,\eta)_{xy} \\ \sigma(\xi,\eta)_z \end{Bmatrix} - \begin{Bmatrix} \sigma(\xi,\eta)_x^* \\ \sigma(\xi,\eta)_y^* \\ \tau(\xi,\eta)_{xy}^* \\ \sigma(\xi,\eta)_z^* \end{Bmatrix} \right)^{\mathrm{T}} \quad (13)$$
$$\left( \begin{Bmatrix} \sigma(\xi,\eta)_x \\ \sigma(\xi,\eta)_y \\ \tau(\xi,\eta)_{xy} \\ \sigma(\xi,\eta)_z \end{Bmatrix} - \begin{Bmatrix} \sigma(\xi,\eta)_x^* \\ \sigma(\xi,\eta)_y^* \\ \tau(\xi,\eta)_{xy}^* \\ \sigma(\xi,\eta)_z^* \end{Bmatrix} \right) t^e \det J^e d\xi d\eta$$
$$= \sum_{p=1}^{3} \left( \begin{Bmatrix} \sigma(\xi_p,\eta_p)_x \\ \sigma(\xi_p,\eta_p)_y \\ \tau(\xi_p,\eta_p)_{xy} \\ \sigma(\xi_p,\eta_p)_z \end{Bmatrix} - \begin{Bmatrix} \sigma(\xi_p,\eta_p)_x^* \\ \sigma(\xi_p,\eta_p)_y^* \\ \tau(\xi_p,\eta_p)_{xy}^* \\ \sigma(\xi_p,\eta_p)_z^* \end{Bmatrix} \right)^{\mathrm{T}}$$
$$\left( \begin{Bmatrix} \sigma(\xi_p,\eta_p)_x \\ \sigma(\xi_p,\eta_p)_y \\ \tau(\xi_p,\eta_p)_{xy} \\ \sigma(\xi_p,\eta_p)_z \end{Bmatrix} - \begin{Bmatrix} \sigma(\xi_p,\eta_p)_x^* \\ \sigma(\xi_p,\eta_p)_y^* \\ \tau(\xi_p,\eta_p)_{xy}^* \\ \sigma(\xi_p,\eta_p)_z^* \end{Bmatrix} \right) t^e \det J^e W_p$$

and similarly

$$\|\hat{\mathrm{e}}\|^2 = \frac{1}{m} \sum_{e=1}^{m} \sum_{p=1}^{3} \left( \begin{Bmatrix} \sigma(\xi_p,\eta_p)_x \\ \sigma(\xi_p,\eta_p)_y \\ \tau(\xi_p,\eta_p)_{xy} \\ \sigma(\xi_p,\eta_p)_z \end{Bmatrix} \right)^{\mathrm{T}} \quad (14)$$
$$\left( \begin{Bmatrix} \sigma(\xi_p,\eta_p)_x \\ \sigma(\xi_p,\eta_p)_y \\ \tau(\xi_p,\eta_p)_{xy} \\ \sigma(\xi_p,\eta_p)_z \end{Bmatrix} \right) t^e \det J^e W_p$$

where $t^e$ is the thickness of the element for a plane stress case and $t^e = 1$ is the plane strain case. Consequently, the relative stress norm error $\zeta_e$ for each item is considerably <5%, which is acceptable for many applications in engineering. Thus,

$$\zeta_e = \frac{\|e\|_e}{\|\hat{e}\|} \leq \zeta \quad (15)$$

and the new element relative stress error level is identified as a permissible error by:

$$\varepsilon_e = \frac{\|e\|_e}{\zeta \|\hat{e}\|} \leq 1 \quad (16)$$

This means each element with $\varepsilon_e$ is required to be refined and the new size of the mesh needs to be expected. Here the asymptotic convergence rate criteria are implemented, which presume:

$$\|e\|_e \propto h_e^p \quad (17)$$

where $p$ is the approximation of polynomial order. In this study, $p = 2$ since the quadratic polynomial is used for the calculation of FEs. Thus, the new element estimated size is:

$$h_N = \frac{1}{\sqrt{\varepsilon_e}} h_e \tag{18}$$

Depending on the user numbers of refinement, the existing mesh will be considered as the new background mesh and the advancing front method will be replicated. The element type was triangular with six nodes.

# 4. Results and discussion

## 4.1. Cracked plate with four holes

As illustrated in Figure 4, a four holes' rectangular plate of 10 mm diameter and a 6 mm long edge crack is analyzed. The dimensions of the plate are 100 mm × 100 mm × 10 mm. The plate is supported on the bottom and is subjected to a tension force of 10 MPa. The plate is made of aluminium 7075-T6, whose properties are shown in Table 1.

Table 1. Mechanical properties of aluminium 7075-T6 [51]

| Property | Value in metric unit |
|---|---|
| Modulus of elasticity, E | 72 GPa |
| Poisson's ratio, $\upsilon$ | 0.33 |
| Yield strength, $\sigma_y$ | 469 MPa |
| Ultimate strength, $\sigma_u$ | 538 MPa |
| Fracture toughness, $K_{IC}$ | 3,288.76 MPa $\sqrt{mm}$ |

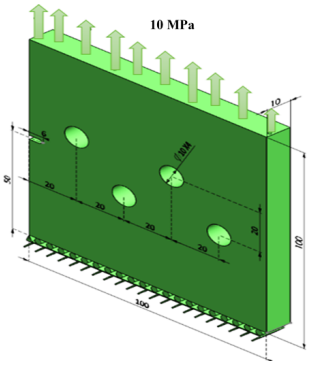
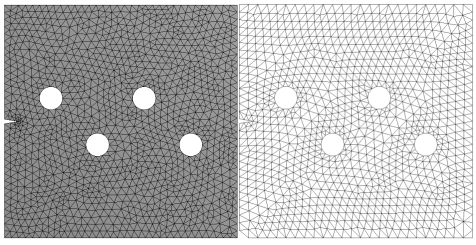



Fig. 4. Cracked plate with four holes and one edge crack.

The geometry is fixed in the x and y directions at the bottom face in the developed program, while in Ansys the geometry is fixed in the x, y, and z directions.

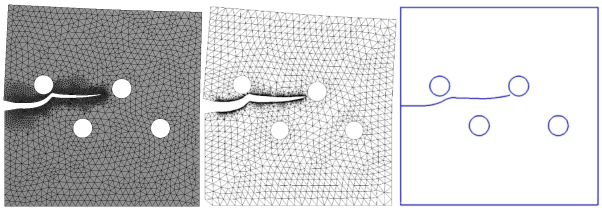
The meshed geometry created in Ansys workbench has 14,737 nodes and 7,177 elements, while the meshed geometry generated in the developed program has 3,933 nodes and 1,911 elements, as represented in Figure 5.



(A) (B)

Fig. 5. Initial generated mesh **(A)** Ansys Workbench, **(B)** developed program.

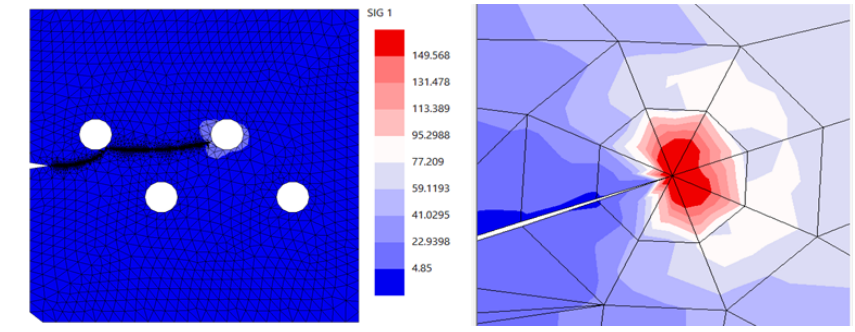
The predicted crack growth paths in both software is shown in Figure 6, and these were also in good agreement with that path predicted by Knowles and Sternberg [51] using the fast multipole method (FMM) boundary element method.



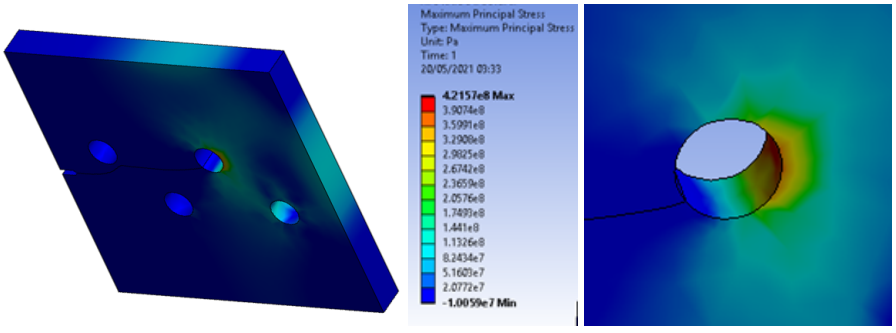
(A) (B) (C)

Fig. 6. Crack growth path: **(A)** Ansys Workbench, **(B)** developed program, **(C)** FMM backscattered electron macroscope (BEM) [46]. FMM, fast multipole method.

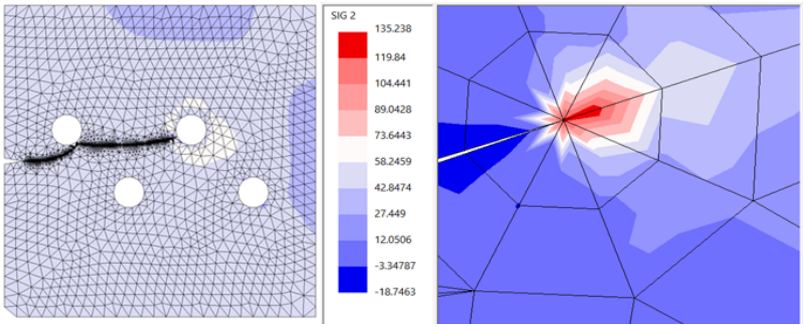
The maximum and minimum principal stresses were compared side by side in both programs, as represented in Figure 7. In Figure 7, the crack starts to grow in a straight line as there is no influence of any holes. As it approaches the hole, the path propagates towards the hole. The crack deviated its direction because the first upper hole was not close



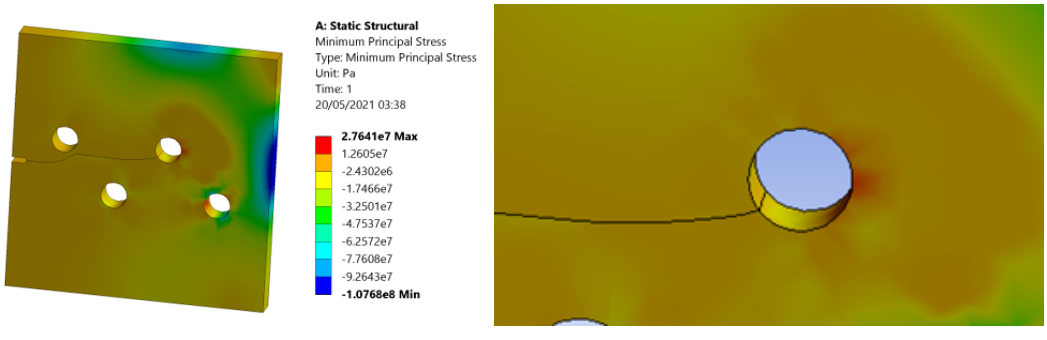

(A)




(B)




(C)




(D)

Fig. 7. Crack growth trajectory **(A)** maximum principal stress (developed program), **(B)** maximum principal stress (Ansys), **(C)** minimum principal stress (developed program), **(D)** minimum principal stress (Ansys). All units in MPa.

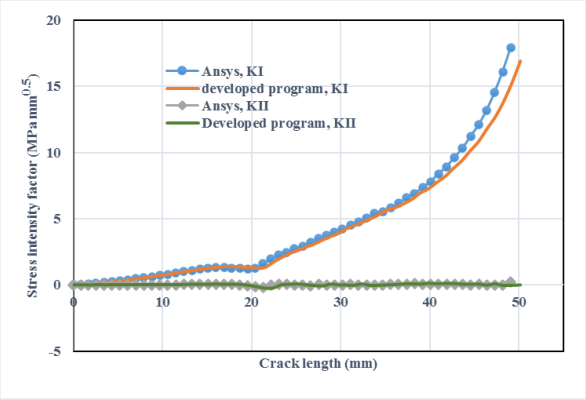
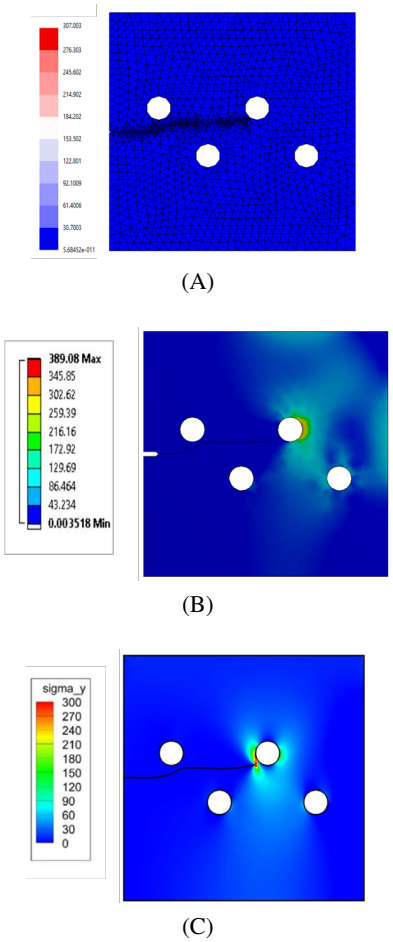



Fig. 8. $K_I$ and $K_{II}$ for cracked plate with four holes.




(A)

(B)

(C)

Fig. 9. Comparison for the stress contour distribution in y direction **(A)** developed program, **(B)** Ansys, and **(C)** FMM BEM [52]. All units in MPa. FMM, fast multipole method.

enough to attract the crack to sink in the hole. It continued to propagate in a straight line up until it reached near the second upper hole, close enough to the crack trajectory so that the crack sinks into this hole. The predicted estimation of the mixed-mode stress intensity parameters $K_I$ and $K_{II}$ are depicted in Figure 8. These estimation values accurately represented the crack growth trajectory. The values of the first mode of SIFs decreased in the interval of the crack length between 15 mm and 20 mm consequent to the influence of the first upper hole. In contrast, the second mode of stress intensity factor increased slightly for the same interval, as Figure 8 shows. As the crack trajectory missed the first upper hole, the value of $K_I$ starts to increase again until the crack reached the second upper hole.

Figure 9 shows the comparison for the stress contour distribution in y direction between the developed program results, Ansys results, and the results obtained by Knowles and Sternberg [51] using FMM boundary element method.

## 4.2. Three holes single edge cracked plate

A more complex mixed-mode crack growth problem was investigated to illustrate the performance of the developed program to represent the propagation of cracks from beginning notches in a three holes single edge cracked plate and precisely prognosticate the values of SIFs. The geometry of three holes single edge cracked plate, and its final adaptive mesh, is presented in Figure 10. This case was investigated for the first time by Ingraffea

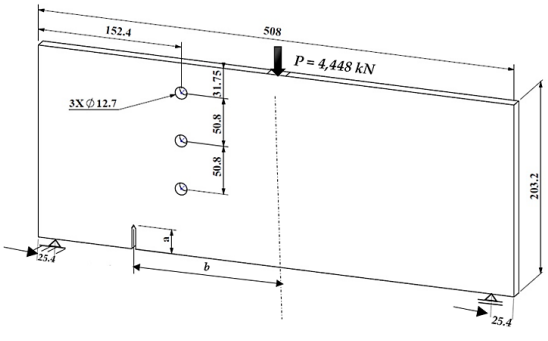
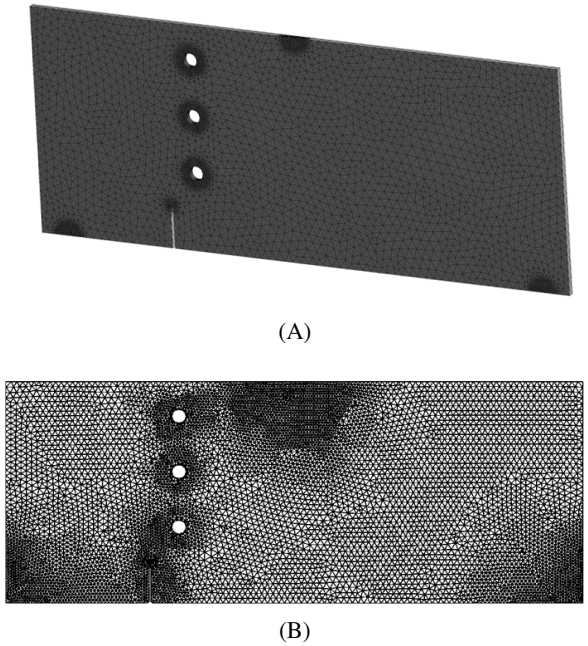



Fig. 10. Geometry and boundary condition of the three holes' single edge crack plate.

and Grigoriu [53]. The results revealed that small changes in the crack path's initial position significantly impacted the results. As a benchmark for numerical models, this example is commonly used to assess the system's predictive abilities. As indicated in Table 2, the geometry analyzed has 2L = 508 mm, width = 203.2 mm, and thickness = 12.7 mm, with two alternative configurations depending on the initial crack length and position. The initial meshes for this geometry, generated by the developed program and Ansys before starting the simulation, are shown in Figure 11.

Table 2. Configurations of the three holes' single edge cracked plate

| Specimen No. | Length of crack, a (mm) | Crack position, b (mm) |
|---|---|---|
| 1 | 25.4 | 152.4 |
| 2 | 38.1 | 127 |



(A)

(B)

Fig. 11. Initial mesh of the three holes' single edge cracked plate in **(A)** Ansys, **(B)** developed program.

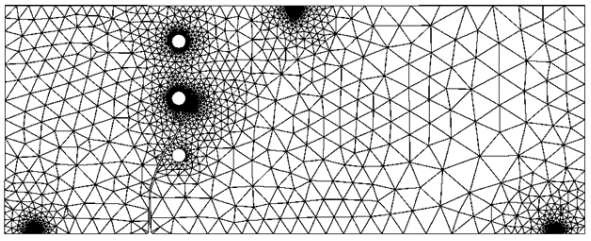
The length of the crack in the first configurations is $a_o$ = 25.4 mm, and it is positioned at a distance of b = 152.4 mm from the mid-length of the beam. The second configuration differs from the first by having an initial crack length of $a_o$ = 38.1 mm, and it is positioned at a distance of b = 127 mm. The specimen is subjected to a cyclic point load at the upper mid-span position with a force of 4,448 kN. The material properties are shown in Table 3.

Table 3. Mechanical properties of the three holes single edge cracked plate [22]

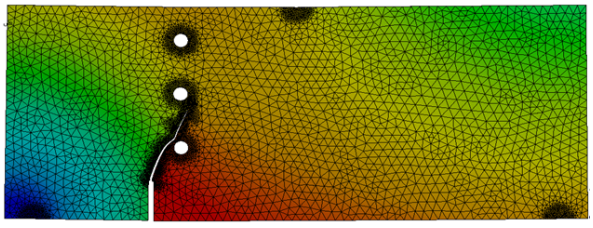
| Properties | Metric units value |
|---|---|
| Modulus of elasticity, $E$ | 205 GPa |
| Poisson's ratio, $\upsilon$ | 0.3 |
| Yield strength, $\sigma_y$ | 516 MPa |
| Fracture toughness, $K_{IC}$ | 730 MPa $\sqrt{m}$ |
| Threshold SIF, $\Delta k_{th}$ | 80 MPa $\sqrt{\text{mm}}$ |
| Paris' law coefficient, $C$ | $1.2 \times 10^{-11}$ |
| Paris law exponent, $m$ | 3 |

Specimens are constrained to all degrees of freedom from the left pin position, similar to the experimental specimen. In contrast, the correct pin only has a first degree of freedom of translation UX. For the first configuration of specimen number one, the simulated crack propagation using the developed program and Ansys software is shown in Figure 12 with an identical crack growth trajectory. The crack growth trajectory goes between the lower and middle holes in this specimen and approaches the middle hole from the right side. It implies that the shear stress intensity factor (KII) surrounding the holes has significantly increased, forcing the crack step-sizes to be decreased.

The crack trajectory using the developed program and Ansys ends up in excellent agreement with experimental data presented in the literature [47, 48], numerical results using the coupled extended meshfree-smoothed meshfree method presented by Knowles and Sternberg [51], and XFEM results obtained by Zhang and Tabiei [21]. Numerical results obtained by Kanth et al. [14] using a polygonal XFEM with numerical integration as shown in Figure 13 A, B, C, D, E, and F, respectively.

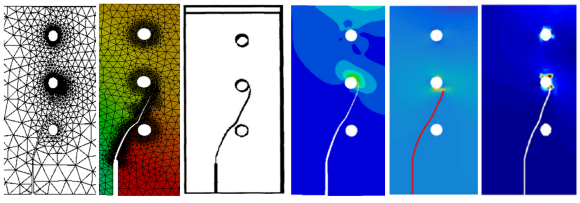


(A)



(B)

Fig. 12. Predicted crack growth path for specimen 1, **(A)** developed program, **(B)** Ansys.



(A) (B) (C) (D) (E) (F)

Fig. 13. Specimen 1, crack growth trajectory **(A)** Ansys simulation **(B)** developed program **(C)** experimental [53], **(D)** numerical results [54], **(E)** numerical results [22], **(F)** numerical results [15].

The results of this simulation for dimensionless stress factors by using the developed program and Ansys are shown in Figure 14, which are almost identical to each other. As can be seen in this figure, the SIFs increase in magnitude as the crack approaches the hole, demonstrating the hole's influence on the crack trajectory. For the second configuration of specimen number two, the simulated crack propagation using the developed program and Ansys software is shown in Figure 15 with an almost identical crack growth trajectory. The crack in this specimen propagates above the lower hole to the middle hole's left side.

Figure 16 depicts the direction of crack growth

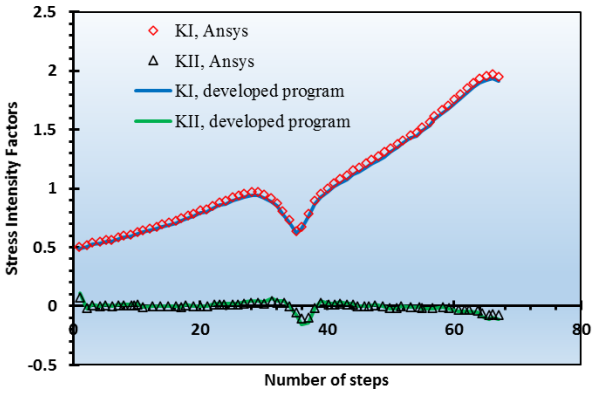
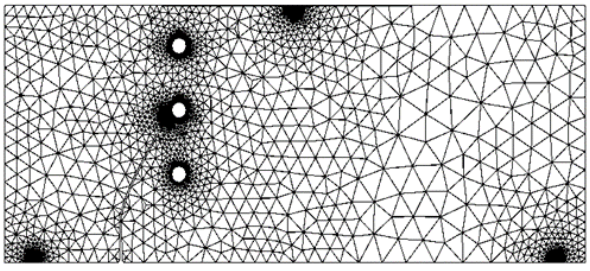
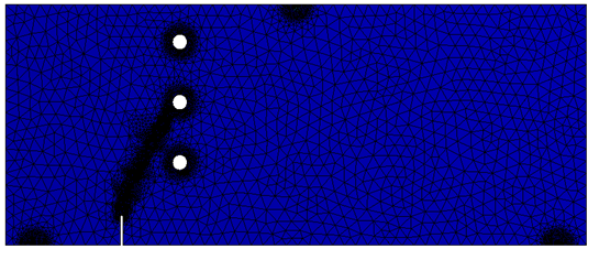



Fig. 14. Dimensionless SIFs for specimen 1. SIFs, stress intensity factors.



(A)

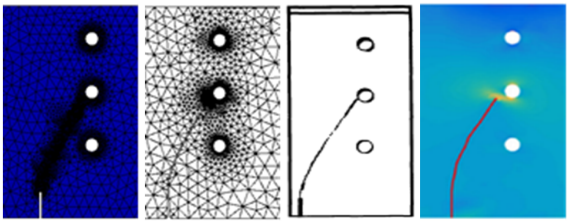


(B)

Fig. 15. Predicted crack growth path for specimen 2, **(A)** developed program, **(B)** Ansys.

for specimen 2, which was compared to the experimental crack trajectory performed in the literature [47, 48] and the numerical findings utilizing the coupled expanded meshfree-smoothed meshfree technique provided by Knowles and Sternberg [51], as illustrated in Figure 16 A, B, C, and D respectively.

The predicted values of the two modes of SIFs in the developed program and Ansys are depicted in Figure 17 with excellent agreement. As observed in the figure, the lower hole has no influence on the



(A) (B) (C) (D)

Fig. 16. Specimen 1, crack growth trajectory, **(A)** Ansys simulation, **(B)** developed program, **(C)** experimental [53, 55], **(D)** numerical results [54].

crack growth direction, since the initial crack was far from the lower hole, while the middle hole has a stronger influence, attracting the crack to sink into the hole.

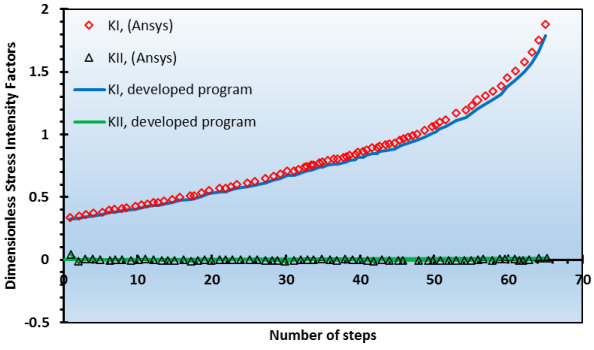



Fig. 17. Dimensionless SIFs for specimen 2. SIFs, stress intensity factors.

## 5. Conclusions

Regarding the simulation results of two- and three-dimensional analysis using the developed program and Ansys software, a satisfactory agreement was obtained between numerical and experimental crack propagation growth trajectories for the simulated specimens. However, for the first geometry there was a differential between the 2D and 3D $K_I$ values that were related to the mesh density variation. Both software's predicted fatigue life was based on Paris law, and all findings were in excellent agreement with each other. The presence of the hole in the plate influences the crack. It alters the crack trajectory to the hole. Based on the position of the hole, the crack growth trajectory will either deviate from the hole, which is known as the missed hole phenomena, or grow toward the hole and sink within, which is known as the sink in the hole phenomena. The two-dimensional analysis takes less computational time than the three-dimensional analysis and produces a fine mesh similar to the three-dimensional one due to available computational capabilities.

The three-dimensional simulation is preferable to the two-dimensional simulation to visualize better stresses, strains, deformation, and many other characteristics, despite the two-dimensional representation being sufficient.

## References

[1] Al Laham S, Branch SI. Stress intensity factor and limit load handbook. Gloucester, Volume 3. UK: British Energy Generation Limited; 1998.

[2] Tada H, Paris PC, Irwin GR, Tada H. The stress analysis of cracks handbook, Volume 130. New York

[3] Sih, G.; Liebowitz, H. Mathematical Fundamentals. In Fracture, Academic Press New York: 1968; Vol. 2, pp. 67-190.

[4] Hellan K. Introduction to fracture mechanics. McGraw-Hill; New York, 1985.

[5] Barsom J, Rolfe S. Fracture and fatigue in structure: Application of fracture mechanics. Philadelphia, PA: American Society for Testing and Materials; 1999.

[6] Hasan, S.; Akhtar, N. Dugdale model for three equal collinear straight cracks: An analytical approach. *Theoretical and Applied Fracture Mechanics* **2015**, *78*, 40-50.

[7] Hasan, S.; Akhtar, N. Mathematical model for three equal collinear straight cracks: A modified Dugdale approach. *Strength, Fracture and Complexity* **2015**, *9*, 211-232.

[8] Kumar S, Singh I, Mishra B, Singh A. New enrichments in XFEM to model dynamic crack response of 2-D elastic solids. Int J Impact Eng. 2016;87:198–211.

[9] Pandey V, Singh I, Mishra B, Ahmad S, Rao AV, Kumar V. A new framework based on continuum damage mechanics and XFEM for high cycle fatigue crack growth: ASME Press; 2000.

[10] Alshoaibi AM, Fageehi YA. 2D finite element simulation of mixed mode fatigue crack propagation for CTS specimen. J Mater Res Technol. 2020;9:7850–61.

[11] Li X, Li H, Liu L, Liu Y, Ju M, Zhao J. Investigating the crack initiation and propagation mechanism in brittle rocks using grain-based finite-discrete element method. Int J Rock Mech Min Sci. 2020;127:104219.

[12] Leclerc W, Haddad H, Guessasma M. On the suitability of a discrete element method to simulate cracks initiation and propagation in heterogeneous media. Int J

Solids Struct. 2017;108:98–114.
[13] Shao Y, Duan Q, Qiu S. Adaptive consistent element-free Galerkin method for phase-field model of brittle fracture. Comput Mech. 2019;64:741–67.
[14] Kanth SA, Harmain G, Jameel A. Modeling of nonlinear crack growth in steel and aluminum alloys by the element free galerkin method. Mater Today Proc. 2018;5:18805–14.
[15] Huynh HD, Nguyen MN, Cusatis G, Tanaka S, Bui TQ. A polygonal XFEM with new numerical integration for linear elastic fracture mechanics. Eng Fract Mech. 2019;213:241–63.
[16] Surendran M, Natarajan S, Palani G, Bordas SP. Linear smoothed extended finite element method for fatigue crack growth simulations. Eng Fract Mech. 2019;206:551–64.
[17] Rozumek D, Marciniak Z, Lesiuk G, Correia J. Mixed mode I/II/III fatigue crack growth in S355 steel. Procedia Struct Integr. 2017;5:896–903.
[18] Dekker R, van der Meer F, Maljaars J, Sluys L. A cohesive XFEM model for simulating fatigue crack growth under mixed-mode loading and overloading. Int J Numer Methods Eng. 2019;118:561–77.
[19] Rezaei S, Wulfinghoff S, Reese S. Prediction of fracture and damage in micro/nano coating systems using cohesive zone elements. Int J Solids Struct. 2017;121:62–74.
[20] Xu W, Wu X. Weight functions and strip-yield model analysis for three collinear cracks. Eng Fract Mech. 2012;85: 73–87.
[21] Zhang W, Tabiei A. An efficient implementation of phase field method with explicit time integration. J Appl Comput Mech. 2020;6:373–82.
[22] Dirik H, Yalçinkaya T. Crack path and life prediction under mixed mode cyclic variable amplitude loading through XFEM. Int J Fatigue. 2018;114:34–50.
[23] Demir O, Ayhan AO, İriç S. A new specimen for mixed mode-I/II fracture tests: Modeling, experiments and criteria development. Eng Fract Mech. 2017;178:457–76.
[24] Zhang R, Guo R. Determination of crack tip stress intensity factors by singular Voronoi cell finite element model. Eng Fract Mech. 2018;197:206–16.
[25] Belytschko T, Black T. Elastic crack growth in finite elements with minimal remeshing. Int J Numer Methods Eng. 1999;45:601–20.
[26] Bergara A, Dorado J, Martin-Meizoso A, Martínez-Esnaola J. Fatigue crack propagation in complex stress fields: Experiments and numerical simulations using the Extended Finite Element Method (XFEM). Int J Fatigue. 2017;103:112–21.
[27] Demir O, Ayhan AO, Sedat I, Lekesiz H. Evaluation of mixed mode-I/II criteria for fatigue crack propagation using experiments and modeling. Chinese J Aeronaut 2018;31:1525–34.
[28] Sajith S, Murthy K, Robi P. Experimental and numerical investigation of mixed mode fatigue crack growth models in aluminum 6061-T6. Int J Fatigue. 2020;130:105285.
[29] Alshoaibi AM. Finite element procedures for the numerical simulation of fatigue crack propagation under mixed mode loading. Struct Eng Mech. 2010;35:283–99.
[30] Alshoaibi AM. Comprehensive comparisons of two and three dimensional numerical estimation of stress intensity factors and crack propagation in linear elastic analysis. Int J Integr Eng. 2019;11:45–52.
[31] Fageehi YA, Alshoaibi AM. Numerical simulation of mixed-mode fatigue crack growth for compact tension shear specimen. Adv Mater Sci Eng. 2020;1-14. https://doi.org/10.1155/2020/5426831
[32] Chen H, Wang Q, Zeng W, Liu G, Sun J, He L, et al. Dynamic brittle crack propagation modeling using singular edge-based smoothed finite element method with local mesh rezoning. Eur J Mech A Solids 2019;76:208–23.
[33] Gomes G, Miranda AC. Analysis of crack growth problems using the object-oriented program bemcracker2D. Frattura ed Integrità Strutturale 2018;12:67–85.
[34] Fageehi YA, Alshoaibi AM. Nonplanar crack growth simulation of multiple cracks using finite element method. Adv Mater Sci Eng. 2020; 1-12.
[35] Alshoaibi AM. Numerical modeling of crack growth under mixed-mode loading. Appl Sci. 2021;11:2975.
[36] Paris P, Erdogan F. A critical analysis of crack propagation laws; J. Basic Eng. Dec 1963, 85(4): 528-53337.
[37] Coffin L. Cyclic deformation and fatigue of metals. Fatigue and Endurance of Metals [Russian translation], Moscow; 1963. 257–72.
[38] Wöhler A. Versuche zur Ermittlung der auf die Eisenbahnwagenachsen einwirkenden Kräfte und die Widerstandsfähigkeit der Wagen-Achsen. Zeitschrift für Bauwesen. 1860;10:583–614.
[39] Bjørheim F. Practical comparison of crack meshing in ANSYS mechanical APDL 19.2. Norway: University of Stavanger; 2019.
[40] Erdogan F, Sih G. On the crack extension in plates under plane loading and transverse shear. J Basic Eng. 1963;85:519–525.
[41] Hussain M, Pu S, Underwood J. Strain energy release rate for a crack under combined mode I and mode II. In Proceedings of the Fracture analysis: Proceedings of the 1973 national symposium on fracture mechanics, Part II; West Conshohocken, PA, 1974.
[42] Nuismer R. An energy release rate criterion for mixed mode fracture. Int J Fract. 1975;11:245–50.
[43] Lee Y-L, Pan J, Hathaway R, Barkey M. Fatigue testing and analysis: Theory and practice, Volume 13. Burlington, Mass.: Butterworth-Heinemann,2005.
[44] Irwin GR. Analysis of stresses and strains near the end of a crack transversing a plate. Trans ASME Ser E J Appl Mech. 1957;24:361–4.
[45] Bashiri AH, Alshoaibi AM. Adaptive finite element prediction of fatigue life and crack path in 2D structural components. Metals. 2020;10:1316.
[46] Rice JR. A path independent integral and the approximate analysis of strain concentration by notches and cracks. J Appl Mech. 1968;35:379–86.

[47] Alshoaibi AM. Finite element simulation of fatigue life estimation and crack path prediction of two dimensional structures components. HKIE Trans. 2013;15:1–6.
[48] Alshoaibi AM. An adaptive finite element framework for fatigue crack propagation under constant amplitude loading. Int J Appl Sci Eng. 2015;13:261–70.
[49] Alshoaibi AM. A two dimensional simulation of crack propagation using adaptive finite element analysis. J Comput Appl Mech. 2018;49:335.
[50] Alshoaibi AM, Hadi M, Ariffin A. Two-dimensional numerical estimation of stress intensity factors and crack propagation in linear elastic analysis. Struct Durability Health Monit. 2007;3:15.
[51] Knowles JK, Sternberg E. On a class of conservation laws in linearized and finite elastostatics. California Institute of Technology, Pasadena Division of Engineering and Applied Science; 1971.
[52] Liu Y, Li Y, Xie WJ. Modeling of multiple crack propagation in 2-D elastic solids by the fast multipole boundary element method. Eng Fract Mech. 2017;172:1–16.
[53] Ingraffea AR, Grigoriu M. Probabilistic fracture mechanics: A validation of predictive capability. Cornell University Ithaca, NY, Department of Structural Engineering; 1990.
[54] Ma W, Liu G, Wang W. A coupled extended meshfree – Smoothed meshfree method for crack growth simulation. Theor Appl Fract Mech. 2020;107:102572.
[55] Bittencourt T, Wawrzynek P, Ingraffea A, Sousa J. Quasi-automatic simulation of crack propagation for 2D LEFM problems. Eng Fract Mech. 1996;55:321–34.

*Received 2021-09-03*
*Accepted 2021-10-07*